Metal–Organic Frameworks

Deutsche Ausgabe: DOI: 10.1002/ange.201604023
Internationale Ausgabe: DOI: 10.1002/anie.201604023

Precise Modulation of the Breathing Behavior and Pore Surface in Zr-MOFs by Reversible Post-Synthetic Variable-Spacer Installation to Fine-Tune the Expansion Magnitude and Sorption Properties

*Cheng-Xia Chen, Zhangwen Wei, Ji-Jun Jiang, Yan-Zhong Fan, Shao-Ping Zheng, Chen-Chen Cao, Yu-Hao Li, Dieter Fenske, and Cheng-Yong Su**

Abstract: *To combine flexibility and modifiability towards a more controllable complexity of MOFs, a post-synthetic variable-spacer installation (PVSI) strategy is used to implement kinetic installation/ uninstallation of secondary ligands into/from a robust yet flexible proto-Zr-MOF. This PVSI process features precise positioning of spacers with different length, size, number, and functionality, enabling accurate fixation of successive breathing stages and fine-tuning of pore surface. It shows unprecedented synthetic tailorability to create complicated MOFs in a predictable way for property modification, for example, CO_2 and R22 adsorption/separation, thermal/chemical stability, and extended breathing behavior.*

The booming progress in the field of metal–organic frameworks (MOFs) has taken advantage of versatile combinations of organic and inorganic synthetic strategies, and in turn, propelled synthetic chemistry into a new realm for precise control over multiplicity and complexity.[1] The syntheses of MOFs have featured generation of permanent porosity,[2] construction of flexible and dynamic frameworks,[3] and has now reached post-synthetic modification (PSM) capability.[4] Flexible MOFs have triggered great interest in soft porous crystals[2a] displaying dynamic response to the external stimuli,[5] resulting in a breathing effect that is tunable at the molecular level to induce more functionality. For example, a systematic tuning of the framework flexibility and gas sorption has been accomplished via combining a library of functionalized linkers as mixed-components.[6] Nevertheless, rational fine-tuning of responsiveness of flexible MOFs is still desired but challenging,[6] and precise control of breathing behavior and fixation of swelling magnitude at stepwise stages have not been achieved to the best of our knowledge.

On the other hand, the PSM methods provide a powerful way to modify and create new functionalities, which are often unattainable by direct de novo synthesis.[4b,7] Specifically, the PSM approach is useful to introduce multiple functionalities into MOFs through sequential post-synthetic ligand exchange,[8] offering an alternative to the one-pot synthesis of MTV-MOFs (multivariate MOFs)[9] to place multiple components, thus avoiding random distribution and disorder.[9b] However, it is noticeable that these PSM routes are mainly limited to post-modifications on the main framework of parent MOFs. Recently, Zhou et al.[10] established an unique sequential linker installation (SLI) strategy to construct MTV-MOFs with exact positioning of multiple linkers, and insertion of secondary ligands for pore space partition and locking has also been accomplished.[11] Nevertheless, these post-syntheses still demand size- and symmetry-matching of inserted ligands with primary frameworks. Insertion of variable secondary ligands into the parent MOFs remains unexplored, which may be expected to create more sophisticated materials.[1]

Based on the above progress in synthetic chemistry, we herein propose a stepwise yet kinetically reversible synthetic approach, that is, post-synthetic variable-spacer installation (PVSI) strategy as depicted in Scheme 1, which presents unprecedented control and tuning capacity through precise and pinpoint installation and uninstallation of different spacers. Starting from a flexible proto-MOF $[(Zr_6(\mu_3\text{-}O)_8(H_2O)_8(L^1)_4]\cdot$(solvents) (LIFM-28, L^1 = 2,2′-bis (trifluoromethyl)-4,4′-biphenyldicarboxylate, LIFM = Lehn Institute

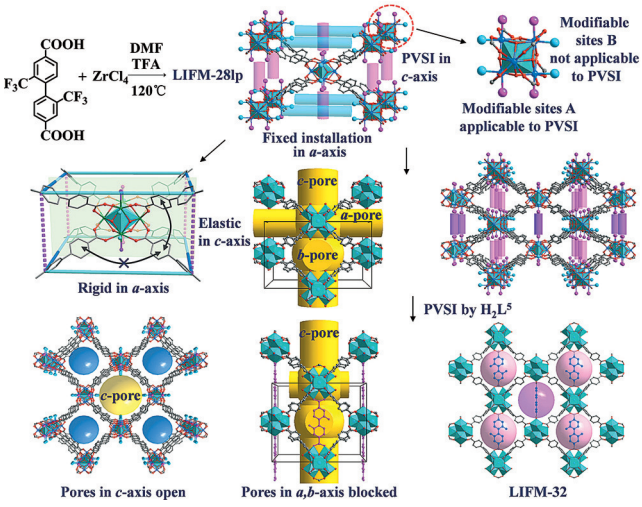

Scheme 1. Post-synthetic variable-spacer installation (PVSI) demonstration by spacer H_2L^5. Elastic deformation occurring in the *c*-axis is controllable by spacers of different lengths. H atoms and CF_3 groups are omitted for clarity.

[*] C.-X. Chen, Z. W. Wei, J.-J. Jiang, Y.-Z. Fan, S.-P. Zheng, C.-C. Cao, Y.-H. Li, Prof. D. Fenske, Prof. C.-Y. Su
MOE Laboratory of Bioinorganic and Synthetic Chemistry
Lehn Institute of Functional Materials
School of Chemistry and Chemical Engineering
Sun Yat-Sen University, Guangzhou 510275 (China)
E-mail: cesscy@mail.sysu.edu.cn

Supporting information and the ORCID identification number(s) for the author(s) of this article can be found under: http://dx.doi.org/10.1002/anie.201604023.

of Functional Materials), insertion of predetermined spacers of variable lengths and substituents at selected sites proceeds facilely through single-crystal to single-crystal (SC-SC) transformations under mild conditions. Therefore, this strategy is applicable to both flexible and post-modifiable MOFs by comprising framework dynamics and modifiable sites, offering an easy way to precisely modulate the breathing behavior by fixing the swelling framework at variate stages to a large extent, and simultaneously modifying the pore surface for improved fluorocarbons and CO_2 adsorption and separation capacity.

To implement the PVSI strategy for dynamic MOFs, a linear ligand $\mathbf{H_2L^1}$ was designed, which bears two trifluoromethyl groups at 2,2′-positions to twist two phenylcarboxylate moieties off a plane. This ligand configuration is essential for construction of 8-connected ***bcu*** framework based on Zr_6-cluster,[12] and may endow the framework with flexibility.[6,13] As expected, colorless crystals were obtained through solvothermal reaction of $ZrCl_4$ and $\mathbf{H_2L^1}$ in *N*,*N*-dimethylformamide (DMF) at 120 °C, giving LIFM-28 as an isostructure of PCN-700 with required network.[10] The as-prepared LIFM-28 crystallizes in $P4_2/mmc$ group (Supporting Information, Table S1), possessing a neutral framework with most probably octahedral $Zr_6O_8(H_2O)_8$ clusters[14] bridged by eight $\mathbf{L^1}$ ligands while leaving four pairs of terminal H_2O groups at equatorial plane appropriate for further modification (Scheme 1; Supporting Information, Figure S4). The crystal lattice presents two types of pores, smaller ones (atom-to-atom separation 7×13 and 7×6 Å^2) along the *a*- or *b*-axis (*a*- or *b*-pores), and larger ones (17×17, 10×10 Å^2) along the *c*-axis (*c*-pores). The CF_3 functional groups point to the interior of the channels to bring hydrophobic character (Supporting Information, Figure S4). A striking feature of LIFM-28 is the breathing behavior driven by removal/uptake of solvated water, which is rarely observed for Zr-MOFs.[5g,13] Upon heating at 100 °C, the crystals transform into a denser phase with the pore size along *a*/*b*-axis dramatically reduced from 7.2 to 3.6 Å (Scheme 2; Supporting Information, Figures S5, S6), showing negative thermal expansion.[5f] When soaking the shrinked crystals in water or acid/basic aqueous solutions, they recover to the original phase readily. This structural transformation takes place in a SC-SC manner, designated as the narrow-pore (LIFM-28np) and large-pore (LIFM-28lp) forms. Taking advantage of this breathing effect, we find that different spacers with varied lengths can be installed or uninstalled through a reversible SC-SC way in mild post-synthetic conditions, thus facilitating PVSI process based on this dynamic proto-Zr-MOF.

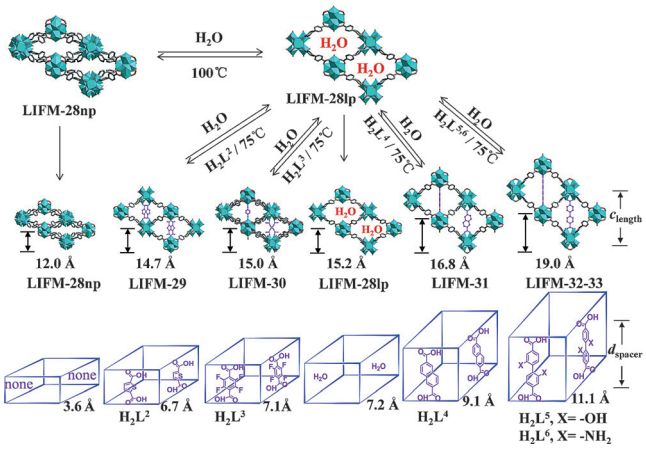

Scheme 2. Reversible breathing behavior of LIFM-28, and stepwise installation/ uninstallation of spacers ($\mathbf{L^2}$–$\mathbf{L^6}$) in an increasing sequence of expansion magnitude.

Careful examination of the Zr_6-cluster in LIFM-28 reveals that 8 terminal waters are located in two types of crystallographically independent positions in orthogonal directions, assigning to modifiable sites **A** and **B** (Scheme 1). Since the Zr_6 cluster lies on a 4_2 screw axis, four H_2O on sites **A** aligning on *c*-axis point to the center of smaller pores along *a*- and *b*-axis (sites **A** in *a*- and *b*-direction are crystallographically equivalent but rotated by 90° and slid by half a *c* vector), while four H_2O on sites **B** aligning on the *a*- or *b*-axis point to the center of larger pores along the *c*-axis. Therefore, the smaller spacing between adjacent sites **A** can accommodate shorter linear dicarboxylate spacers to replace four H_2O, thus blocking *a*- and *b*-pores (Scheme 1; Supporting Information, Figure S5), while longer spacers fitting between two neighboring sites **B** will partition *c*-pores into segmental domains.[10] As illustrated in Scheme 1, the dihedral angle of diphenyl linkers facing *c*-axis is stretchable because they chelate three facial Zr atoms on one face of octahedral Zr_6 cluster, but that facing *a*-axis is relatively rigid because of unbending fixation by three meridional Zr atoms on a Zr_6 octahedron. Consequently, the framework is able to self-adjust the spacing between sites **A** to install spacers in the *c*-direction with variable length, meanwhile little altering the separation between sites **B** in the *a*- and *b*-directions. In other words, the framework can breathe in the *c*-direction while keeping the size of *c*-pores almost unchanged. This unique structural attribute lays the foundation of PVSI strategy, namely, applying installation on sites **A** to enable elastic deformation along *c*-axis depending on the size of the spacers, but preventing installation on sites **B** to purposely remain *c*-pores for functional modification. PVSI presents an alternative functionalization pathway evolving from SLI method[10] in which two types of linkers with mutual matching length have been successfully positioned in two distinct pockets of prototype PCN-700 in a fixed-order sequence. The SLI strategy is preferable for MTV-MOFs with mixed linkers, but nevertheless blocking pores in all directions. The PVSI strategy aims at control of flexibility and selection of installation sites, and features: i) the enabling of fine-tuning of framework swelling magnitude by insertion of spacers of different length in the same direction; ii) leaving free pores for practical utilizations such as gas adsorption; iii) modifying the surface of the main empty pores via installation of functional spacers bearing varied substituents; and iv) enhancing thermal stability and BET specific surface. It is worthy to note that PVSI modification actually changes the topology of parent framework after spacer coordination; however, such post-synthetic coordination is labile enough to undergo solvent-assisted ligand exchange,[7,10] probably owing to the low activation energy for kinetic replacement of H_2O by carboxylate spacers in neutral form without altering overall charge of proto-MOF.

To check if the proto-MOF LIFM-28 is robust enough for repeating and successive PVSI processes, the chemical stability of LIFM-28 has been tested under harsh conditions. PXRD indicates that the structure remains intact upon immersion in boiling water and aqueous solutions at pH 1 and 12 at 100 °C (Supporting Information, Figure S7). These results confirm that the proto-LIFM-28 is highly stable to maintain the framework against solution treatment (noting that phase change always occurs from LIFM-28np to LIFM-28lp in aqueous media, and vice versa under activation conditions). Therefore, PVSI process has been fully tested with continually elongating spacers covering a wide range. The spacing between adjacent sites **A** (designating as d_{spacer}) in LIFM-28 is 3.6 Å in its np-form, becoming 7.2 Å in its lp-form, while the spacing between neighboring sites **B** is 16.3 Å. As analyzed above, because the spacing between sites **B** is rather rigid, so installation of spacer shorter than 16 Å will inevitably select sites **A**. Along this line, two shorter spacers, $\mathbf{H_2L^2}$ and $\mathbf{H_2L^3}$ with d_{spacer} falling within the range between np-form and lp-form of LIFM-28, and three longer spacers, $\mathbf{H_2L^4}$, $\mathbf{H_2L^5}$, and $\mathbf{H_2L^6}$ with d_{spacer} significantly longer than the spacing in LIFM-28lp, have been chosen for PVSI testing (Scheme 2). As an example, fresh LIFM-28lp crystals were immersed in a DMF solution of $\mathbf{H_2L^2}$ at 75 °C for 24 h, leading to formation of LIFM-29 incorporating a $\mathbf{H_2L^2}$ spacer with $\mathbf{L^1}$:$\mathbf{L^2}$ ratio of 2:1. This means four H_2O on neighboring sites **A** can be kinetically replaced by two immigrating spacers to generate a topologically new framework. All other spacers can undergo similar PVSI process to generate isoreticular MOFs of LIFM-30 ($\mathbf{H_2L^3}$), LIFM-31 ($\mathbf{H_2L^4}$), LIFM-32 ($\mathbf{H_2L^5}$), and LIFM-33 ($\mathbf{H_2L^6}$), with spacers positioned exactly between sites **A** (Scheme 2). The structures of all single crystals produced via PVSI have been determined (Supporting Information, Figure S4, Table S1). Treatments of the spacer-installed crystals with water or acid/basic aqueous solution lead to uninstallation of the spacers (Supporting Information, Figures S8–S12) to recover LIFM-28lp, except LIFM-33, which is apt to collapse under basic conditions, probably because of the NH_2 group. The phase purity of PVSI products has been verified by PXRD measurements (Supporting Information, Figures S14–S18). ^{1}H and ^{19}F NMR spectral analyses of the digested LIFM-29–33 in comparison with starting LIFM-28lp reveal that two spacers per Zr_6 cluster are installed in LIFM-29 and LIFM-33, while only one spacer is installed in LIFM-30–32 (Supporting Information, Figures S19–S25, Table S2), in agreement with the single-crystal analysis results.

The elastic deformation effect induced by PVSI of different spacers can be evaluated by the crystal expansion magnitude along *c*-axis (c_{length}), and the specific volume derived from the unit cell volume (V_{cell}) and the number of formula per unit cell (Z) in the single crystal ($V_{specific\ volume} = V_{cell}/Z$), taking the densest LIFM-28np as the reference (Figure 1). It is clear that, in comparison with the shortest spacing between sites **A** in LIFM-28np, the spacer elongation from $\mathbf{H_2L^2}$ (186 %) to $\mathbf{H_2L^6}$ (316 %) causes crystal expansion along *c*-axis from 123 % to 159 %, and swelling of the specific volume from 119 % to 136 %. In contrast, the pore size in *c*-direction only shrinks less than 10 %. Taking the structural

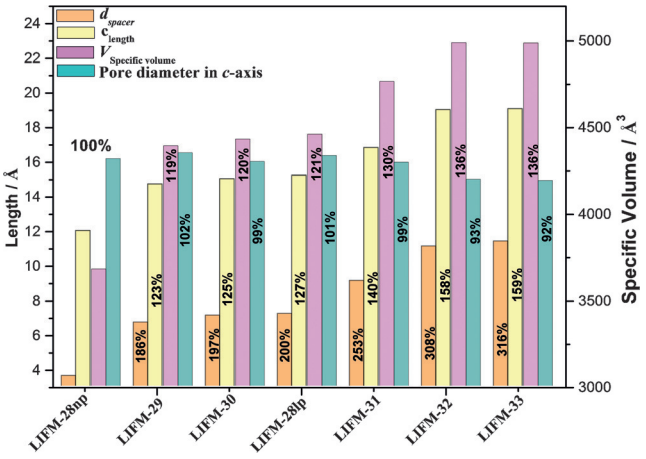

Figure 1. Comparison of elastic deformation depending on the size of spacer (d_{spacer}), crystal expansion magnitude along *c*-axis (c_{length}), and specific volume ($V_{specific\ volume}$) relative to LIFM-28np, and changes of pore size along the *c*-axis.

change between np-form and lp-form of LIFM-28 into consideration, it is evident that two shorter spacers ($\mathbf{H_2L^2}$ and $\mathbf{H_2L^3}$) leads to contraction with regard to the original LIFM-28lp, while three longer spacers ($\mathbf{H_2L^4}$, $\mathbf{H_2L^5}$, and $\mathbf{H_2L^6}$) result in expansion significantly surpassing the breathing magnitude driven by water solvent. Such a modulation of breathing effect by spacer installation is unprecedented and impressive, especially the extra expansion beyond the ordinary breathing behavior driven by external stimuli.[2a,3,5] Moreover, installation of different spacers is a precise control of the breathing behavior by fixing the swelling framework at variate stages.

To testify the reversibility of the PVSI process, uninstallation and reinstallation of the inserted spacers have also been fully performed in the following sequence (Supporting Information, Figures S26–S45): i) soaking the crystal of LIFM-29–33 in water at room temperature for a certain time (1 h to 3 days); ii) checking the phase and chemical change of the soaked crystal with single-crystal X-ray diffraction, PXRD, and ^{1}H and ^{19}F NMR spectroscopy; and iii) reinstalling the spacers verified by PXRD and ^{1}H NMR. As expected, the single-crystal and powder X-ray analyses unambiguously confirm that the water-soaked crystals transform back into LIFM-28lp. ^{1}H and ^{19}F NMR monitoring of the digested samples of soaked and reinstalled crystals verify that the inserted spacers in LIFM-29–33 are completely removed or reinstalled. Further confirmation comes from gas sorption examination of the activated crystals recovered from LIFM-30 (Supporting Information, Figure S46). Its sorption isotherms closely match the profile with the pristine LIFM-28np, evidently indicative of full recovery of the porosity and complete removal of spacers along reversible PVSI process. These phenomena strongly suggest that PVSI is a kinetically controlled process via labile coordination between the inserted spacers and Zr_6 clusters, in contrast to conventional one-pot synthetic and post-synthetic approaches, facilitating reversible installation/uninstallation of spacers and efficient recycling of the proto-MOF. In this sense, a continuous cycle starting from the most compressed LIFM-28np to the most

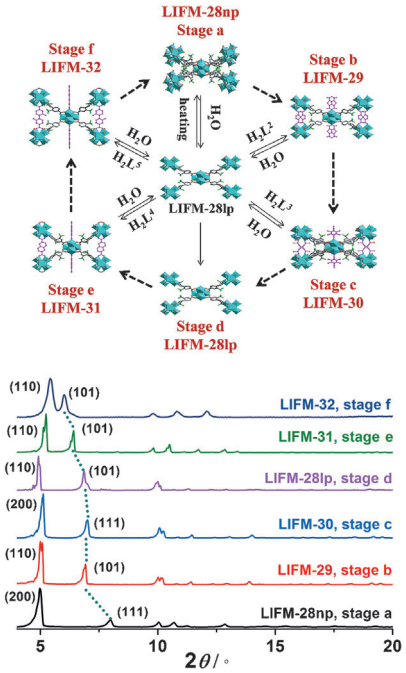

Figure 2. Top: Stepwise installation/uninstallation from H_2L^2 to H_2L^5 mediated by reversible PVSI processes with LIFM-28lp crystals to achieve different stages of breathing behaviors in a continuous way. Bottom: Elastic deformation in six stages reflected by specific PXRD peaks shift.

expanded LIFM-32 (Figure 2 top, shown by the broken arrow) through every stage fixed by spacers is feasible via reversible mediation by LIFM-28lp (shown by equilibrium arrows). Since the structural transformation between np- and lp-forms of LIFM-28 is facially driven by water uptake, the key steps rely on the robustness of LIFM-28lp to endure successive PVSI processes with different spacers. Therefore, an experiment is designed to install H_2L^2-H_2L^5 step-by-step with the same LIFM-28lp crystals. As shown in the Supporting Information, Figure S47, stepwise installation and uninstallation of these spacers has been successfully accomplished, where each PVSI step involves a process of spacer insertion and LIFM-28lp recovery, which is testified by PXRD monitoring (Supporting Information, Figure S48). In this way, fixation of the breathing behavior at six stages could be established, and the crystal elastic deformation along *c*-axis could be precisely determined by the values of d_{spacer} and c_{length} mentioned above, and reflected on the movement of the PXRD peaks containing non-zero Miller *l*-indice of a crystal plane (Figure 2; Supporting Information, Figure S49). Furthermore, the robustness of LIFM-28 against spacer insertion/removal has been testified by ten cycles of reversible PVSI processes with H_2L^5, indicating little crystal degrading occurs, as seen from PXRD monitoring (Supporting Information, Figure S50).

On the other hand, PVSI of different spacers into *a*- and *b*-pores in LIFM-28lp will simultaneously modify the surface of the purposely remained *c*-pores. Anchoring the thiophene ring in H_2L^2, tetrafluorophenyl motif in H_2L^3, naphthalene aromatics in H_2L^4, hydroxy group in H_2L^5, and amino groups in H_2L^6 on the surface of *c*-pores may bring potential interacting/coordinative sites or hydrophobic/hydrophilic effect into the porous framework. The position and number of post-modified spacers can be predictably and accurately determined; therefore, fine-tuning of the pore properties is possible. In general, all MOFs show good thermal and chemical stability owing to existence of F-functionalized L^1 carboxylate ligand[15] and oxophilic Zr_6-cluster. Thermogravimetric analyses indicate that the frameworks decompose above 300 °C, increasing variably depending on the introduced spacers (Supporting Information, Figure S51). The variable-temperature PXRD patterns of LIFM-28lp confirm that the structural transformation to LIFM-28np occurs around 100 °C, and retains the crystallinity up to 200 °C. After PVSI of different spacers, the framework stability increases significantly up to 375 °C for LIFM-29, 425 °C for LIFM-30, and 350 °C for LIFM-32, while remaining unchanged for LIFM-31 and LIFM-33 (Supporting Information, Figures S52–S57), indicative of best enhancement from F-substituents. At higher temperature, severe broadening of PXRD patterns indicates collapse of the porous framework. Owing to labile spacer coordination, LIFM-29–33 are thermodynamically unstable and undergo uninstallation of kinetic spacers in water and acidic/basic aqueous solutions (Supporting Information, Figures S8–S12), but remain stable afterwards.

The N_2 sorption was performed at 77 K for all MOFs, which display typical type-I isotherms with BET surface area increasing from 940 in LIFM-28lp to 1588 $m^2 g^{-1}$ in LIFM-33 (Supporting Information, Figures S58–S66, Table S3). The pore volume, estimated at $p/p_0 = 0.97$, also increases from 0.44 to 0.76 $cm^3 g^{-1}$, while the pore sizes fall in a similar range around 13 Å. These results are expectable since insertion of flat spacers into smaller *a*/*b*-pores should generally expand the overall specific surface areas along the main *c*-pores. Slight variation of BET surface area and pore volume is due to distinct functionalization of spacer substituents. It is impressive that the modified MOFs show much higher adsorption capacity and selectivity for chlorodifuoromethane (R22) and CO_2 (Supporting Information, Figures S67–S98, Table S4). At zero coverage, the R22 isosteric heat Q_{st} ranges from 26 to 36 kJ mol^{-1} (Supporting Information, Figure S86). The highest value is from LIFM-30 containing fluorinated spacers, being comparable with the best values reported.[15] Moreover, excellent R22 adsorption selectivity over N_2 has been achieved by the modified MOFs. Ideal adsorption solution theory (IAST) calculation reveals that the initial selectivities of LIFM-29–33 falls in the range 170–279, which is a significant improvement by a factor of 4–7 from 42 of LIFM-28lp (Figures 3 left, Supporting Information, Figures S87–S98, Table S4). For CO_2, introducing NH_2 groups in LIFM-33 remarkably enhance CO_2 uptake capacity due to very high Q_{st} of about 40 kJ mol^{-1}, followed by LIFM-32 bearing OH sites and then other modified MOFs (Supporting Information, Figure S85, Table S4). Again, the CO_2/N_2 adsorption selectivities of the post-installed MOFs are distinctly higher than that of LIFM-28lp (Figure 3 right), reaching highest value of about 30 by LIFM-33.

In summary, we have demonstrated a post-synthetic variable-spacer installation (PVSI) strategy based on a stable

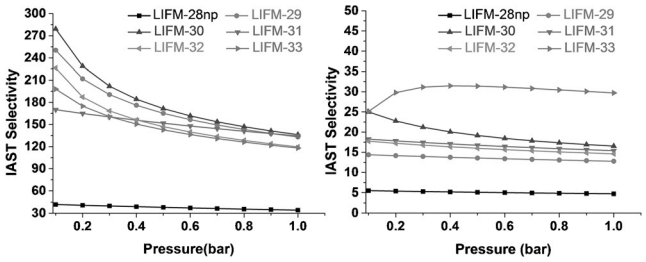

Figure 3. IAST calculative selectivity of R22/N_2 (10:90, left) and CO_2/N_2 (15:85, right) at 273 K.

yet flexible proto-Zr_6-MOF LIFM-28, which features SC-SC structural transition between a narrow-pore (np) and a large-pore (lp) phases driven by solvent water uptake. Through this strategy, a series of multifuctional MOFs are generated via pinpoint replacement of the selected terminal H_2O molecules on a Zr_6 cluster by linear spacers with different lengths and substituents. The PVSI process is kinetically reversible in mild conditions, providing a versatile alternative to conventional PSM and one-pot syntheses by enabling exact positioning of length-variable spacers in the same location. Therefore, assembly and disassembly of different spacers through PVSI approach endows a facile way not only to precisely control the breathing behavior by fixing the elastic deformation in a stepwise manner beyond normal external stimuli, but also to fine-tune the pore surface to improve gas sorption capacity and separation ability, enlarge BET surface area, and stabilize the overall framework.

Acknowledgements

This work was supported by the 973 Program (2012CB821701), the NSFC Projects (91222201, 21573291), the STP Project of Guangzhou (15020016), and the NSF of Guangdong Province (S2013030013474).

Keywords: breathing effect · metal–organic frameworks · post-synthetic modification · R22 adsorption · spacer insertion

How to cite: *Angew. Chem. Int. Ed.* **2016**, *55*, 9932–9936
Angew. Chem. **2016**, *128*, 10086–10090

[1] a) H. Furukawa, K. E. Cordova, M. O'Keeffe, O. M. Yaghi, *Science* **2013**, *341*, 974; b) H. Furukawa, U. Muller, O. M. Yaghi, *Angew. Chem. Int. Ed.* **2015**, *54*, 3417–3430; *Angew. Chem.* **2015**, *127*, 3480–3494.

[2] a) S. Horike, S. Shimomura, S. Kitagawa, *Nat. Chem.* **2009**, *1*, 695; b) J. Liu, L. Chen, H. Cui, J. Zhang, L. Zhang, C. Su, *Chem. Soc. Rev.* **2014**, *43*, 6011–6061.

[3] A. Schneemann, V. Bon, I. Schwedler, I. Senkovska, S. Kaskel, R. A. Fischer, *Chem. Soc. Rev.* **2014**, *43*, 6062–6096.

[4] a) S. M. Cohen, *Chem. Rev.* **2012**, *112*, 970–1000; b) Z. Wang, S. M. Cohen, *Chem. Soc. Rev.* **2009**, *38*, 1315–1329.

[5] a) D. N. Dybtsev, H. Chun, K. Kim, *Angew. Chem. Int. Ed.* **2004**, *43*, 5033–5036; *Angew. Chem.* **2004**, *116*, 5143–5146; b) S. Bourrelly, P. L. Llewellyn, C. Serre, F. Millange, T. Loiseau, G. Férey, *J. Am. Chem. Soc.* **2005**, *127*, 13519–13521; c) G. Férey, C. Serre, *Chem. Soc. Rev.* **2009**, *38*, 1380–1399; d) A. Boutin, D. Bousquet, A. U. Ortiz, F.-X. Coudert, A. H. Fuchs, A. Ballandras, G. Weber, I. Bezverkhyy, J.-P. Bellat, G. Ortiz, G. Chaplais, J.-L. Paillaud, C. Marichal, H. Nouali, J. Patarin, *J. Phys. Chem. C* **2013**, *117*, 8180–8188; e) Y. Liu, J.-H. Her, A. Dailly, A. J. Ramirez-Cuesta, D. A. Neumann, C. M. Brown, *J. Am. Chem. Soc.* **2008**, *130*, 11813–11818; f) H.-L. Zhou, Y.-B. Zhang, J.-P. Zhang, X.-M. Chen, *Nat. Commun.* **2015**, *6*, 6917; g) Q. Zhang, J. Su, D. Feng, Z. Wei, X. Zou, H.-C. Zhou, *J. Am. Chem. Soc.* **2015**, *137*, 10064–10067.

[6] S. Henke, A. Schneemann, A. Wütscher, R. A. Fischer, *J. Am. Chem. Soc.* **2012**, *134*, 9464–9474.

[7] a) O. Karagiaridi, W. Bury, J. E. Mondloch, J. T. Hupp, O. K. Farha, *Angew. Chem. Int. Ed.* **2014**, *53*, 4530–4540; *Angew. Chem.* **2014**, *126*, 4618–4628; b) P. Deria, J. E. Mondloch, E. Tylianakis, P. Ghosh, W. Bury, R. Q. Snurr, J. T. Hupp, O. K. Farha, *J. Am. Chem. Soc.* **2013**, *135*, 16801–16804.

[8] C. Liu, T.-Y. Luo, E. S. Feura, C. Zhang, N. L. Rosi, *J. Am. Chem. Soc.* **2015**, *137*, 10508–10511.

[9] a) H. Deng, C. J. Doonan, H. Furukawa, R. B. Ferreira, J. Towne, C. B. Knobler, B. Wang, O. M. Yaghi, *Science* **2010**, *327*, 846–850; b) L. Liu, K. Konstas, M. R. Hill, S. G. Telfer, *J. Am. Chem. Soc.* **2013**, *135*, 17731–17734; c) H. Chevreau, T. Devic, F. Salles, G. Maurin, N. Stock, C. Serre, *Angew. Chem. Int. Ed.* **2013**, *52*, 5056–5060; *Angew. Chem.* **2013**, *125*, 5160–5164.

[10] S. Yuan, W. Lu, Y. P. Chen, Q. Zhang, T. F. Liu, D. Feng, X. Wang, J. Qin, H. C. Zhou, *J. Am. Chem. Soc.* **2015**, *137*, 3177–3180.

[11] a) S.-T. Zheng, J. T. Bu, Y. Li, T. Wu, F. Zuo, P. Feng, X. Bu, *J. Am. Chem. Soc.* **2010**, *132*, 17062–17064; b) H. Wang, J. Xu, D.-S. Zhang, Q. Chen, R.-M. Wen, Z. Chang, X.-H. Bu, *Angew. Chem. Int. Ed.* **2015**, *54*, 5966–5970; *Angew. Chem.* **2015**, *127*, 6064–6068; c) H. J. Park, Y. E. Cheon, M. P. Suh, *Chem. Eur. J.* **2010**, *16*, 11662–11669.

[12] Y. Bai, Y. Dou, L.-H. Xie, W. Rutledge, J.-R. Li, H.-C. Zhou, *Chem. Soc. Rev.* **2016**.

[13] P. Deria, D. A. Gómez-Gualdrón, W. Bury, H. T. Schaef, T. C. Wang, P. K. Thallapally, A. A. Sarjeant, R. Q. Snurr, J. T. Hupp, O. K. Farha, *J. Am. Chem. Soc.* **2015**, *137*, 13183–13190.

[14] H. Cui, Y. Wang, Y. Wang, Y.-Z. Fan, L. Zhang, C.-Y. Su, *CrystEngComm* **2016**, *18*, 2203–2209.

[15] a) R.-B. Lin, T.-Y. Li, H.-L. Zhou, C.-T. He, J.-P. Zhang, X.-M. Chen, *Chem. Sci.* **2015**, *6*, 2516–2521; b) R. K. Motkuri, H. V. Annapureddy, M. Vijaykumar, H. T. Schaef, P. F. Martin, B. P. McGrail, L. X. Dang, R. Krishna, P. K. Thallapally, *Nat. Commun.* **2014**, *5*, 4368.

Received: April 26, 2016
Revised: June 4, 2016
Published online: July 12, 2016

